CENTER FOR ASTROPHYSICS
HARVARD & SMITHSONIAN

# Submillimeter Array Newsletter

Number 41, January 2026

## CONTENTS

1 From the Director

SCIENCE HIGHLIGHTS:

2 The Nature, Internal Structure and Stability of GMCs in M31

9 Measuring the Magnetic Field of the White Dwarf Pulsar AR Sco

12 Pinched Magnetic Fields in the Accreting High-mass Protocluster W3 IRS5

TECHNICAL HIGHLIGHTS:

15 Commissioning SMA Linear Polarization Calibration in CASA

17 Successful SMA Solar Fringe Test

OTHER NEWS

18 SMA 2026A Semester Call for Proposals

Proposal Statistics for 2025B

19 2025B Track Allocations by Weather Requirement and Configuration

Top-Ranked 2025B Semester Proposals

20 Standard, DDT, Large Scale And Key Projects Observed During 2025A

23 Recent Publications

## FROM THE DIRECTOR

Dear SMA Newsletter readers,

Over the past six months, the Submillimeter Array has undergone a period of transition. Tim Norton, the previous Director, retired at the end of last year. I would like to extend my sincere thanks to Tim for his many years of dedicated service to the Center for Astrophysics as a whole, and to the SMA in particular.

I am pleased to take on the role of Acting SMA Director and to serve the CfA community in this capacity. I am no stranger to Hawai'i, having begun my career with the Hawai'i office of the Academia Sinica Institute for Astronomy and Astrophysics (ASIAA). During my time there, I worked on instrument development for several major facilities, including the Submillimeter Array (SMA), the Y. T. Lee Array (YTLA), the Atacama Large Millimeter/Submillimeter Array (ALMA), and the Greenland Telescope (GLT). I later joined the Harvard & Smithsonian Center for Astrophysics (CfA), where I have held technical leadership roles on projects such as the Next Generation Event Horizon Telescope and the Black Hole Explorer. I currently serve as Manager of Central Engineering at the CfA.

This issue of the newsletter highlights three exciting scientific results obtained with the SMA. The first article, by Charles J. Lada and Jan Forbrich, reports unexpected results from a deep SMA survey of M31 exploiting SMA's broad spectral coverage. The second article, by Paul Barrett and Mark Gurwell, presents SMA polarimetric observations that reveal magnetic field properties of the white dwarf and demonstrate notable similarities between white dwarf emission processes and those of neutron star pulsars. Finally, Huei-Ru Vivien Chen and collaborators present high-resolution SMA observations of magnetic field morphologies in star-forming regions.

In the current semester, the SMA will participate in the Event Horizon Telescope (EHT) "movie" campaign, which will focus on studying time variability in M87. Unlike the typical seven- to ten-day observing campaign, this year's effort will span approximately eight weeks, with two scheduled observing sessions per week. The SMA has been a member of the EHT collaboration since its inception and played a pioneering role in the development of phased-array techniques at millimeter and submillimeter wavelengths.

On the technical front, there were many notable accomplishments during the second half of last year. Among the most significant was the successful demonstration of fringes on the Sun in December 2025 on a single baseline, following upgrades to two antennas, which were necessary to protect cabling routed through the subreflector support structure from the higher temperatures expected during solar observations. Similar upgrades to the remaining antennas are planned for this year following this successful first test. SMA has also developed a new polarization data processing pipeline, replacing the legacy IDL-based reduction method. And on the wSMA front, a second antenna has now received upgraded receivers, with first fringes between two wSMA antennas obtained in September of last year. Over the next six months, we plan to upgrade two additional antennas, with a fifth upgrade slated for the second half of this year. In parallel, several facility upgrades are underway, including replacement of the backup power systems and the cooling unit for both the SMA correlator and the SMA facility. Together, these upgrades will enable more robust and reliable operations in the future.

This truly feels like a happy homecoming for me. I have deeply enjoyed the many years I spent in Hawai'i working alongside friends and colleagues at the SMA, other observatories, and 'Imiloa. I am genuinely excited to be returning, even if it is in an interim role.

*Ranjani Srinivasan*
*Acting Director, Submillimeter Array*

# THE NATURE, INTERNAL STRUCTURE AND STABILITY OF GMCs IN M31

Charles J. Lada[1] & Jan Forbrich[2]

Occasionally, some of the most compelling scientific insights from an astronomical survey emerge from results that were neither foreseen nor explicitly intended in its original design. This article is about one such example, an unexpected and highly significant outcome from a recent large SMA survey of giant molecular clouds (GMCs) in the Andromeda galaxy (M31).

In 2019, we set out to design a survey that would take full advantage of the SMA's newly upgraded wide-band receivers. This upgrade dramatically expanded the array's bandwidth, potentially opening an unprecedented window for detecting and spatially resolving dust continuum emission from individual giant molecular clouds (GMCs) in nearby galaxies. To exploit this new capability, we proposed to image dust emission from a population of GMCs in our nearest large extragalactic neighbor, the Andromeda galaxy (M31). At the time, many considered this an ambitious goal, perhaps even beyond the reach of the SMA. Nevertheless, between 2019 and 2022, we managed to use the upgraded SMA to successfully observe 230 GHz continuum emission in numerous GMCs of M31 (Forbrich *et al.* 2020; Viaene *et al.* 2021). The survey ultimately yielded detections and spatially resolved dust emission maps from a large sample of GMCs within an external galaxy (Bosomworth *et al.* 2026).

The survey was designed to take additional advantage of the upgraded SMA's capability to simultaneously detect CO(J=2-1) emission lines along with the dust continuum emission. As a result, we could not only obtain measurements of the dust masses of individual GMCs, but also calibrate, for the first time, the mass-to-light ratios ($a_{CO}$) for all three CO isotopologues ($^{12}$CO, $^{13}$CO and C$^{18}$O) within the GMC population of a galaxy. Additionally, comparison of the dust and CO emission

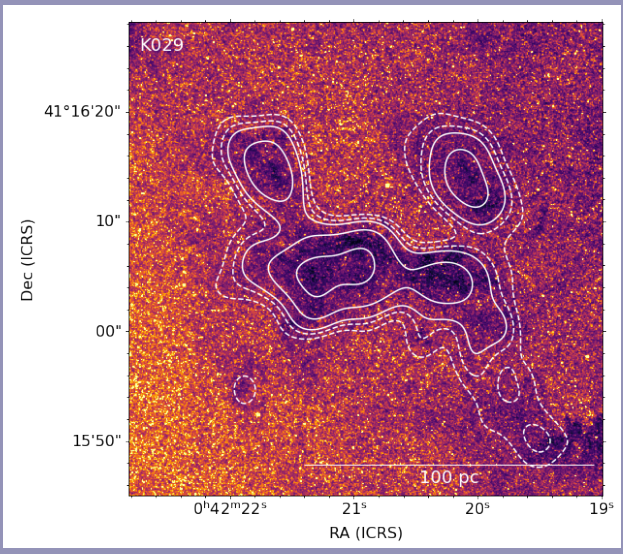


Figure 1: The mass surface density map of the GMCs K029 A and B obtained from $^{12}$CO observations superposed on an optical HST image of the K029 field. This illustrates the close correspondence of the CO emission with the visual extinction produced by the clouds. The outermost contour is the 1 σ boundary and corresponds to a mass surface density of 18 $M_o$ pc$^{-2}$ very close to the expected physical boundary of the molecular clouds. The first solid boundary is the 3 σ boundary of each cloud.

[1]Center for Astrophysics | Harvard & Smithsonian; [2]University of Hertfordshire

enabled direct measurements of the relative abundances of the three CO isotopologues within an extragalactic sample of GMCs. (Viaene *et al.* 2021, Bosomworth *et al.* 2026).

Because the depth of our SMA observations was set to ensure robust dust continuum measurements for individual GMCs in M31, the resulting data achieved exceptionally high signal-to-noise detections of CO emission from all three primary isotopologues. The quality of the spectra was unexpectedly high, far exceeding our initial expectations. In fact, the sensitivity of the observations allowed us to detect and map many more GMCs in CO than in dust emission—only about 25% of the GMCs detected in CO were also detected in dust.

More importantly, the observations were deep enough to trace the full spatial extent of the $^{12}$CO emission from most of the GMCs in the survey as exemplified in Figure 1. This level of sensitivity proved crucial, as the dust emission was typically confined to the dense inner cores of the GMCs and therefore was not useful for characterizing their global properties. In contrast, the deep CO data enabled the derivation of relatively robust, global measurements of the fundamental physical properties of the GMC population, thereby producing a comprehensive inventory of well-constrained sizes, dust-calibrated masses and velocity dispersions of individual GMCs in Andromeda. These measurements, in turn, provided the basis for a deeper investigation into the physical nature of GMCs within M31 than otherwise would have been possible. Describing some of the salient results obtained from the CO observations—including a number of unexpected findings—will be the focus of the rest of this article.

Observing M31 from the outside of that galaxy enabled us to measure GMC physical properties across the entire disk of the galaxy with clarity and uniform precision. This is something not possible for GMCs in the Milky Way, where viewed from within, vary greatly in distance and suffer from severe line-of-sight overlap and confusion, leading to large uncertainties in their measured physical properties. Given this vantage point we can potentially learn things about GMCs in M31 that provide new insights to understanding GMCs in the Milky Way as well.

The global inventory of cloud properties in M31 enabled a comprehensive investigation of Larson's three relations—the mass–size, linewidth–size, and virial relations—originally derived for Milky Way molecular clouds, now examined within in an extragalactic population of GMCs (Lada *et al.* 2024). Below we summarize the key findings.

Analysis of the M31 data revealed a strong mass-size relation for the GMC sample, very similar to that in the Milky Way GMC population. The relation, like in the Milky Way, exhibited an appreciable scatter. As indicated in Figure 2, detailed examination showed that nearly all of this scatter arose from

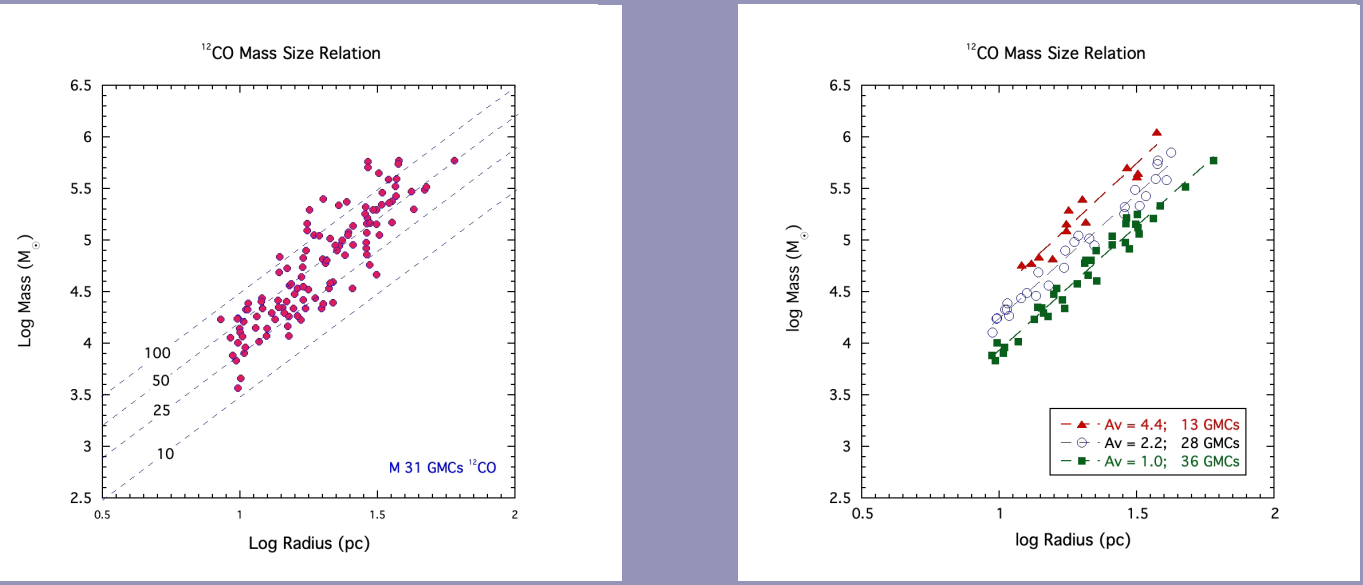


Figure 2: The mass-size relations for the M31 GMCs. On left is the relation for the entire population of clouds. On the right are the mass-size relations for three sets of clouds of different 3σ outer boundaries corresponding to extinctions of 1.0, 2.2 and 4.4 magnitudes. Only GMCs whose boundaries are within 10% of the given boundary are plotted. Lines are least-squares fits to the data. The right plot illustrates the sensitivity of calculated cloud properties (e.g., surface density) to the choice of the adopted cloud boundary (adapted from Lada et al. 2024).

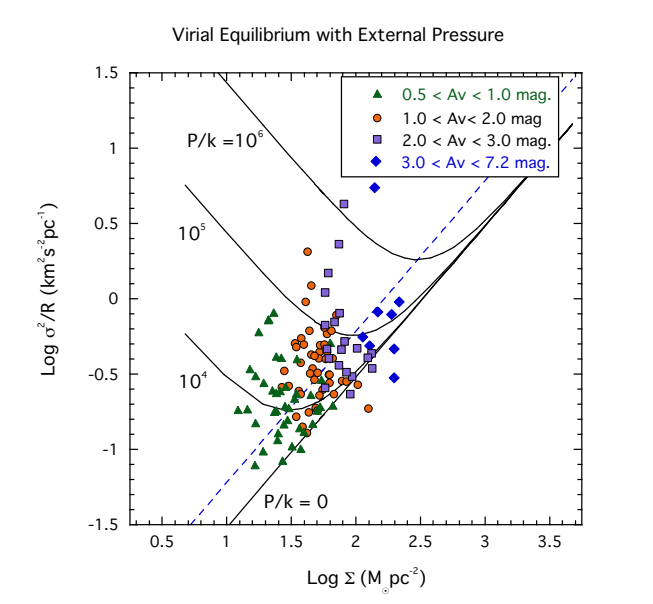


Figure 3: The pressurized viral equilibrium diagram for GMCs in M 31. The solid lines are the theoretically predicted relations for GMCs in virial equilibrium with external surface pressure for different values of the external pressure (i.e., p/k = 0, $10^4$, $10^5$ and $10^6$). Data are color-coded by the value of the 3σ boundary surface density used to define each cloud. The required pressure for confinement spans a range of approximately two orders of magnitude and appears to be positively correlated with the cloud's outer boundary surface density which is set by the image sensitivity. (From Lada et al. 2025).

variations in the empirically determined boundary surface densities used to define the clouds in M31.

In our analysis, the boundary of each GMC was set at the 3σ rms noise level of the interferometric images. Because weather conditions, instrumental sensitivity, and occasional source crowding varied over the four-year survey, the image noise, and hence the adopted surface density threshold boundary for each cloud, was not uniform. These variations introduced artificial differences in the derived GMC surface densities: sources with higher boundary thresholds had systematically higher derived mean surface densities. As a result, these variations in image noise were responsible for most of the apparent scatter in the mass–size relation.

Interestingly, rather than being a limitation, the presence of these variations in the adopted GMC boundaries provided a valuable diagnostic for understanding the underlying nature of the mass–size relation in M31. After correcting for the variations in the mean GMC surface densities introduced by the systematics in cloud definition, the scatter decreased significantly, by roughly a factor of three in dex. This behavior closely mirrors that found for Milky Way clouds (Lombardi *et al.* 2010; Lada & Dame 2020), underscoring the **strong dependence of derived GMC properties on the adopted surface-density threshold that defines their outer boundaries.**

Larson's linewidth-size (LWS) relation was found to be quite weak with a relatively high dispersion in the $^{12}$CO emission lines from M31 GMCs. The slope of the relation is consistent within the uncertainties with that for Milky Way clouds. However, the LWS relation was found to be even weaker and almost non-existent in the $^{13}$CO data for M31, perhaps suggesting a scale dependence for this, the most famous of the Larson relations. If confirmed, this behavior might suggest that the influence of turbulence on cloud dynamics may begin to diminish on larger scales than previously suspected. Similar to the mass-size relation, the LWS relation for M31 GMCs is, within the uncertainties, similar to that for Milky Way clouds, at least in $^{12}$CO.

An initially unexpected result of our analysis emerged from examining Larson's final relation—the virial relation—for the GMC population in M31. Our findings indicated that most M31 GMCs are not in virial equilibrium with approximately 40% of the sample appearing to be gravitationally unbound (Lada *et al.* 2024), contrary to Larson's original results for Milky Way GMCs. However, a more recent study of the Milky Way now shows that a large fraction of its GMCs is also likely unbound (Evans *et al.* 2021). Thus, even in this respect, the M31 clouds closely resemble those in the Milky Way. Overall, in terms of the Larson relations, the GMC populations of M31 and the Milky Way appear essentially indistinguishable in their physical properties.

Perhaps the most surprising and interesting scientific outcome of our survey was the unanticipated and unprecedented information we were able to decipher about the internal spatial structure and dynamical nature of individual GMCs in Andromeda from the CO observations. This resulted from our attempts to better understand why in such a large fraction of M31 GMCs the gravitational and kinetic energies were apparently not in balance.

We posited that all the GMCs were in fact bound or confined by a source of external pressure and not free to expand into M31's ISM. To test this hypothesis and investigate the role of pressure in cloud confinement we plotted the GMCs on the pressurized virial or Keto diagram, first introduced by Keto and Myers (1986). This graph essentially plots the external pressure per unit surface density of a cloud versus its mass surface density and is shown in Figure 3 for a subsample of M31 GMCs characterized by simple, single component gaussian line profiles (termed 1G sources). Solid hyperbolic curves depict the theoretically predicted loci of GMCs in virial equilibrium with surface pressure for different values of

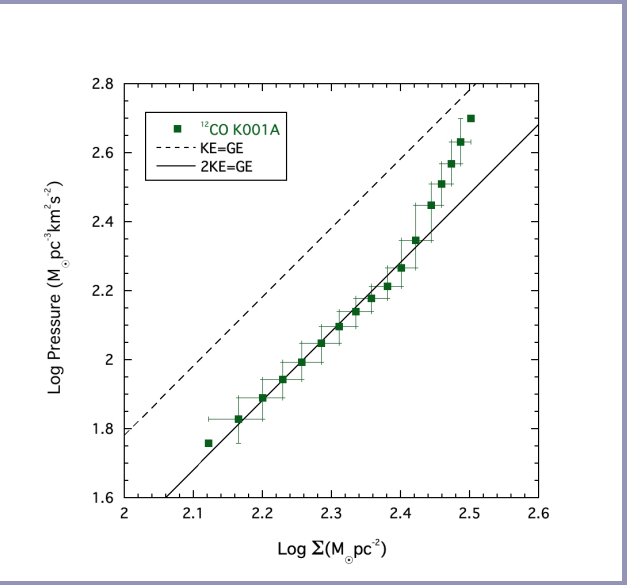


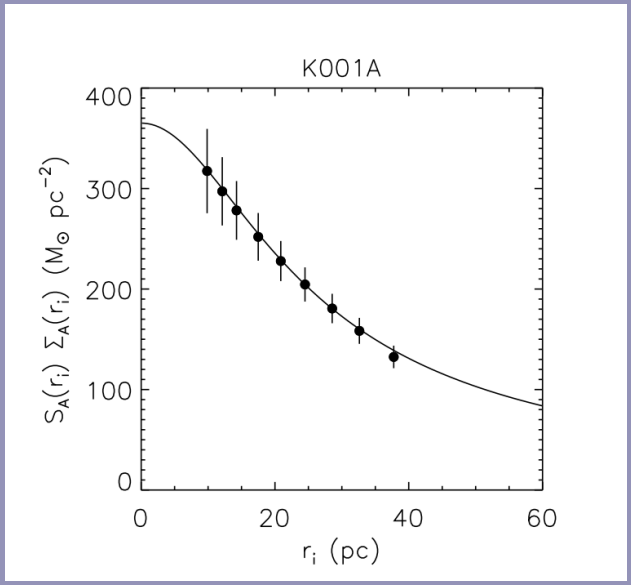


Figure 4: Left: the pressure profile of the GMC K001A along with the virial equilibrium line (solid trace) where the gravitational binding energy (GE) is twice the kinetic energy (KE). The dashed line represents the transition between bound and unbound clouds where KE=GE. At low surface densities the cloud appears to be in virial balance with 2KE = GE across all surface density boundaries. The upward turn in the data at high surface densities marks the region where external pressure provided by outer cloud layers becomes more important than internal gravitational energy for confining the gas. Right: fit of the Lane-Emden equation to the radial surface density profile of K001A (adapted from Keto et al. 2025).

the surface pressure. The dashed linear trace indicates the boundary between bound and unbound clouds (in the absence of external pressure). The behavior of the GMCs on this plot turned out to reveal fundamental new insights into the physical nature of the objects.

As can be seen in Figure 3 a significant GMC fraction appears to be unbound in the absence of an external pressure, corroborating the findings of Lada *et al.* (2024) mentioned above. External pressures ranging from p/k ~ $10^4$ to $10^6$ would be required to ensure that all of the unbound clouds in Figure 2 be in virial equilibrium with, and confined by, an external surface pressure. The most likely source of such external pressure would be the pressure in the mid-plane of the galaxy's disk produced by the weight (including stars and gas) of the disk itself (Elmegreen 1989; Blitz & Rosolowsky 2004). However, the variation of the mid-plane pressure across a disk galaxy like M 31 is an order of magnitude too small to account for the range of pressures required to confine all its clouds (Lada *et al.* 2025).

The average surface density of a GMC is defined by the ratio of its molecular mass to its projected area. This ratio depends sensitively on the empirically adopted outer boundary of the cloud. As noted earlier the M31 cloud boundaries were set by the 3 σ image noise, which varies across the sample. Despite our best efforts to minimize it, the noise induced variation in the defining boundary of a GMC turned out to be a powerful tool for investigating the physical nature of the clouds. In Figure 3 the data are color-coded to indicate the various (3 σ noise fixed) values of surface density used to define the outer boundaries of the clouds in the plot. The location of GMCs on the diagram systematically varies with their adopted outer boundary. This behavior is the key to understanding the nature of this diagram and the sources on it.

GMCs with the lowest boundary (and average) surface densities (green symbols), require the lowest external confining pressures (p/k ~ $10^4$), and these required pressures are comparable to the mid-plane pressure in M31. In contrast GMCs defined by progressively higher boundary surface density require correspondingly higher confining pressures in excess of the mid-plane pressure in order to be virialized. However, for these clouds with higher surface density boundaries our observations were not sufficiently sensitive to detect the material in their outer envelopes. The systematic increase in the inferred external pressure with boundary surface density therefore suggests that **the additional "missing" binding pressure arises from the weight of the undetected molecular gas lying outside the noise-defined boundaries of these clouds.** For these objects we therefore systematically underestimated their total mass and overestimated their average surface densities.

This revelation is remarkable. This is because it suggests that most of the GMCs in M31 are plausibly bound across all internal boundaries, including their outer edges, by a combination of surface pressure and gravity, and that they are in a state of pressurized virial equilibrium throughout their structure.

In their analysis Lada *et al.* (2025) recognized that this intriguing hypothesis could be tested by using the virial diagram in a novel way by performing a differential virial analysis to assess the internal dynamical state of an *individual* GMC. This is illustrated in Figure 4 where a pressure profile of the M31 GMC, K001A is shown. This graph is essentially the Keto diagram modified by plotting the internal pressure of the cloud (i.e., $\Sigma\ \sigma^2/r$), instead of pressure per unit surface density (i.e., $\sigma^2/r$), as a function of the gas surface density within the cloud.

The values of the plotted points are areal averages of the quantities computed over a sequence of increasing boundary surface densities. This sequence begins with the outermost 3σ cloud boundary and increases in 1σ steps until an innermost contour encloses an area comparable to that of the synthesized beam of the interferometer. Specifically, the average surface density, (<Σ>), CO velocity dispersion (σ) and radius (r) are measured for each boundary level in the sequence from spatial averages over the corresponding area enclosed by that boundary level. The radius, r, is defined by the area above the corresponding contour as $r = (A/\pi)^{0.5}$ and thus represents a linear spatial scale representative of the area enclosed by each level in the sequence. This areal approach for defining these observed parameters has the benefit that the derived quantities are independent of cloud geometry. This is particularly advantageous for measurements of GMCs which are generally non-circular and irregularly shaped.

The left panel of Figure 4 shows that the pressure profile of K001A displays a well-behaved, inwardly increasing gradient. At the lower surface densities the pressure displays a smooth linear (power-law) rise with surface density, coincident with the virial equilibrium line within the errors. This behavior suggests that the lower surface density, outer regions of the K001A cloud are in a state of virial balance across every internal boundary or radius. Such a profile is consistent with the theoretical expectations for an object in hydrostatic equilibrium where inward and outward vertical forces are balanced and $p_{internal} \sim \Sigma^2$, independent of cloud shape (Bertoldi & McKee 1992).

This interpretation is reinforced by the right panel of Figure 4, which shows the radial profile of measured surface densities $\Sigma A(r_i)$ for K001A together with a fit to the data of the Lane–Emden equation ($S_A(r_i)$) for hydrostatic equilibrium from Keto *et al.* (2025). The resemblance to the well-studied Milky Way dark cloud B68 is striking: B68's structure is also well described by a Lane–Emden profile (Alves *et al.* 2001; Lada *et al.* 2003). The crucial difference, however, is the physical scale and nature of the pressure support. B68 is a small, isothermal cloud whose internal pressure is dominated by thermal motions (p =nkT), whereas K001A is a much larger and more massive GMC whose internal pressure is dominated by turbulent motions ($p \sim \rho v^2$). In a more relevant comparison, Keto (2024) showed that on larger spatial scales GMCs in the Milky Way also exhibit surface-density profiles that decline with radius in a manner consistent with Lane–Emden predictions. Additionally, as in M31, the Galactic GMCs are governed primarily by turbulent velocities and turbulent pressure.

At the higher surface densities the pressure profile of K001A clearly departs from a single linear relation and the pressure increases more rapidly with surface density. Indeed, the innermost region of the cloud, with the highest surface density, is situated very close to the boundary between bound and unbound objects. Consequently, the internal pressure is very close to exceeding the limit that would enable the inner cloud material to be bound or confined by gravity alone. It seems highly unlikely that the inner parts of this massive GMC are nearly unbound, while the outer regions remain strongly bound and in virial equilibrium. A more plausible explanation is that the inner regions are also in virial equilibrium but confined by the external pressure exerted by the weight of the cloud's outer layers. In other words, the inner regions, which have lower enclosed mass, are not primarily in virial balance between their internal kinetic and gravitational binding energies. Instead, the balance there is maintained by the pressure from the weight of the surrounding cloud layers. Therefore, the GMC maintains virial balance and pressure confinement across its entire structure from the inner regions, held together by a combination of gravity and pressure from the surrounding cloud envelope, to the outer regions confined primarily by gravity and to a lesser extent by external pressure provided by both the general ISM of M31 and the expected, but undetected, atomic hydrogen skin of the cloud (e.g., Elmegreen 1989).

Using our methodology, we constructed internal pressure profiles for 48 M31 GMCs in our sample that have sufficient dynamic range in surface density to insure a minimum of 5 points on the plot. Figure 5 presents these relations, with each GMC shown as a series of data points connected by a solid line. As a group, the GMCs exhibit well-behaved pressure profiles characterized by inwardly increasing pressure gradients, similar to the example of K001A. The profiles are generally parallel to one another and to the virial-equilibrium relation (2KE = GE, or $p_{int} \propto \Sigma^2$). This indicates that, like K001A, most GMCs appear to be in pressure, if not virial, equilibrium across all their boundaries.

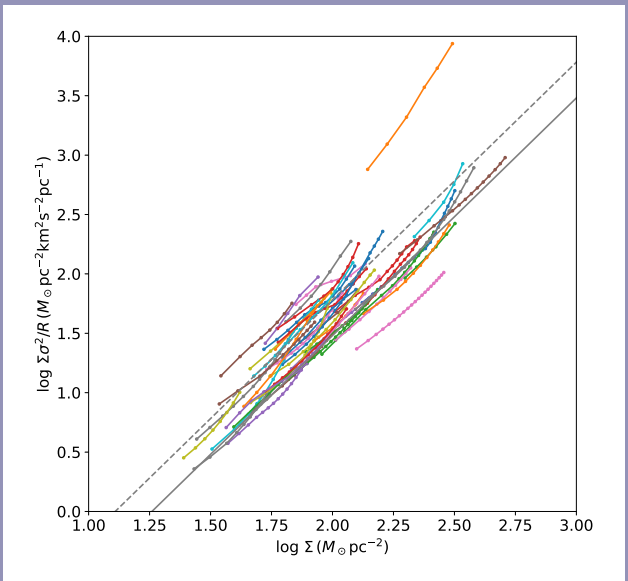


Figure 5: Pressure-Surface relation for 48 GMCs in M31 with significant dynamic range in surface density. The GMCs exhibit well behaved pressure profiles characterized an inwardly increasing pressure gradients. The profiles exhibit a high degree of similarity, being parallel to each other and to the line (solid trace) for pressure-free virial equilibrium (i.e. 2KE=GE and $p \sim \Sigma^2$). From Lada et al. 2025.

Importantly, the shapes of the pressure profiles, and the conclusions drawn from them, are insensitive to the adopted outer cloud boundaries. This contrasts with empirically derived cloud masses, sizes, and corresponding surface densities, which are strongly affected by boundary choices.

The dispersion in the vertical placement of the profiles in Figure 5 is relatively small. Nearly all of this scatter can be explained by the systematic mass-calibration uncertainty associated with the observed variation in the CO-to-mass conversion factor, $\alpha_{CO}$=10±4.5, measured for the SMA GMC sample (Viaene *et al.* 2021) and used to derive the cloud masses here (Lada *et al.* 2024). Consequently, the intrinsic dispersion of the sequence of pressure profiles is even narrower than it appears. The median M31 profile also lies within 1σ of the virial relation, and within the uncertainties most profiles are consistent with virial equilibrium across the entirety of their internal structure.

Many of the profiles in Figure 5 show various degrees of upward displacement at high surface densities, though less striking that for K001A. This upward trend is suggestive of similar physical behavior in the cloud centers, but perhaps more muted due to the relatively low angular resolution of our data. Higher resolution observations would be required to test this possibility.

Another advantage of using a pressure or differential virial diagram to analyze individual GMCs follows from the preceding discussion. In practice it is very difficult to distinguish a bound or virialized GMC from an unbound cloud on such a diagram. This is because the uncertainty in the measurements is dominated by the uncertainty in the CO mass calibration which is on the order of the separation between the expected positions of a virialized and unbound GMC on the diagram. Moreover, the location of the virial line is itself comparably uncertain since it depends on the GMC's gravitational potential, something that is difficult to estimate without detailed knowledge of the three-dimensional mass distribution of a cloud.

In contrast, the relative positions of the points in a pressure profile are accurately known. As demonstrated by Krumholz *et al.* (2025) properties such as the slope, and particularly changes in the slope, can be used in a differential virial analysis to diagnose the overall dynamical state of a cloud. For example, as discussed above, the break and steepening of the slope in the pressure profile of K001A is indicative of an internally stable GMC. Pressure profiles with overall flat or decreasing slopes would be indicative of GMCs in a state of global collapse. Krumholz *et al.* (2025) argued that the predominance of positive slopes in the M31 GMC sample suggests that these GMCs are not undergoing global collapse.

Yet, these GMCs are undergoing star formation, indicating that gravitational collapse is occurring somewhere in the clouds. This is most likely happening in the innermost regions on spatial scales inaccessible to our observations. Construction of pressure profiles using considerably higher angular resolution measurements have the potential to identify the surface densities at which collapse dominates the internal dynamics of a cloud. Such measurements would be very challenging for the GMCs in M31 or any other external galaxy. In the Milky Way such measurements are possible and could be used to determine where the onset of inexorable gravitational collapse occurs.

In summary, what began as an ambitious effort to exploit the SMA's expanded bandwidth for mapping dust continuum emission in Andromeda's GMCs ultimately delivered something more profound from the simultaneously obtained deep CO observations — an unexpected and unprecedented extragalactic view of molecular cloud structure, dynamics, and equilibrium. These observations revealed that M31's GMCs closely mirror those of the Milky Way in their global scaling relations, yet also exposed subtle, previously inaccessible details about how these clouds are confined and internally structured. By leveraging boundary-dependent systematics and introducing a differential virial analyses, the study uncovered compelling evidence that a significant fraction of GMCs

in M31 exist in a state of pressurized virial equilibrium across their full extents—offering a new framework for understanding cloud stability, the role of turbulence, and the conditions that precede star formation. These insights demonstrate the power of sensitive CO observations to continue to deepen our understanding of the physical nature of GMCs. They lay a foundation for future Galactic studies that could reveal where, and how, gravitational collapse truly begins within giant molecular clouds.

In closing, we note that the results of the SMA large program summarized here are based on a series of papers representing the exceptional efforts of various combinations of scientific collaborators, including Glen Petitpas, Sebastien Viaene, Eric Keto, Mark Krumholz, Christopher Faesi, and Chloe Bosomworth. These collaborators made essential contributions across multiple aspects of the project, including planning, data reduction and analysis, observing support, and provision of critical scientific insight into the interpretation of the results. This project would also not have been successful without the dedicated staff of engineers and technicians at the SMA, whose unwavering efforts ensured the facility operated productively, even during the challenging years of the pandemic.

## REFERENCES


- Alves, et al. 2003, Nature, 409, 159
- Bertoldi & McKee, 1992, ApJ, 395, 140
- Blitz & Rosolowsky, 2004, ApJL, 612, L29
- Bosomworth et al. 2026, MNRAS, submitted
- Elmegreen B. 1989, ApJ, 338, 178
- Evans et al. 2021 ApJ, 920, 126
- Forbrich et al. 2020, ApJ 890, 42
- Keto & Myers, 1987, Apj, 304, 466
- Keto, E. 2024, AN, 345, e20240044
- Keto et al. 2025, arXiv:2025.06118
- Krumholz et al. 2025, OJA, 8, 91
- Lada et al. 2003, ApJ, 586, 286
- Lada & Dame 2020, ApJ 898, 3
- Lada et al. 2024, ApJ, 966, 193
- Lada et al. 2025 ApJ, 986, 12
- Larson, R. 1981 MNRAS, 194 809
- Lewis et al. 2021 ApJ, 908, 76
- Lombardi et al. 2010, A&A 519, L7
- Viaene et al. 2021, ApJ, 912, 68

# MEASURING THE MAGNETIC FIELD OF THE WHITE DWARF PULSAR AR SCO

Paul Barrett[1] & Mark Gurwell[2]

The discovery of pulsar-like behavior in the close ($P_{orb}$ = 3.56 hr) white dwarf-red dwarf (WD-RD) binary or cataclysmic variable (CV) AR Sco has firmly demonstrated that WDs can exhibit many of the same characteristics as neutron star pulsars. Marsh *et al.* (2016) were the first to discover highly pulsed (up to 90% pulse fraction) non-thermal emission from the spinning WD in AR Sco, over a wavelength range extending from the radio to the ultraviolet. The binary shows no flickering or flaring at optical wavelengths indicating that the binary is detached and there is no accretion onto the WD, hence the nomenclature of WD pulsar. The pulsations are seen predominantly at 118 s, which is the beating between the 117 s spin period and the 3.56 hr orbital period of the binary. Perhaps the most intriguing aspect of AR Sco is that the bulk of the luminosity of the system is likely the result of the spin-down power of the WD, which is measured to be dP/dt = −(4.82 ± 0.18) x $10^{-17}$ Hz $s^{-1}$ (Gaibor *et al.* 2020). Assuming the bolometric emission is due to magnetic dipole radiation, the magnetic field of the WD is inferred to be ~500 MG. To explain the WD's strong magnetic field and fast spin rate, Schreiber *et al.* (2021) propose that the initial magnetic field of the WD was weak (~1 MG), allowing the WD to be spun up by an accretion disk during an early evolutionary phase of high accretion in the cataclysmic variable. As the WD cooled, its core crystallized causing a convective layer to form, resulting in a rotation-driven dynamo that increased the magnetic field by a factor of ~500. If this scenario is correct, then it should apply to all WDs as they cool and may explain: (1) why WDs become more magnetic as they age (e.g., Bagnulo *et al.* 2022) and (2) why the percentage of magnetic cataclysmic

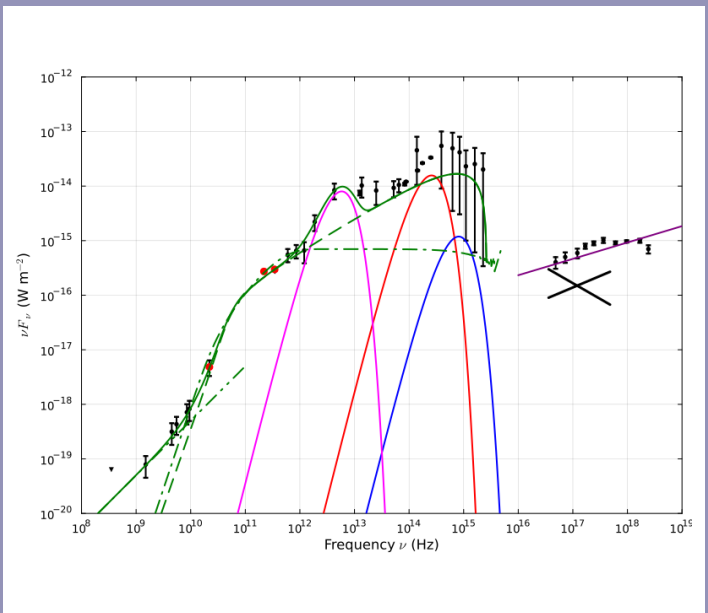


Figure 1: The spectral energy distribution (SED) of AR Sco. Black bars show the range spanned by intensive, time-resolved data. The red square and hexagons are the VLA K band (22 GHz) and Submillimeter Array (SMA) (220 & 345 GHz) data. Black points with error bars (1σ) represent single exposures. The black lines represent the ±1σ range of the X-ray spectral slopes. Triangles are upper limits. The red and blue lines show model atmospheres, extended at long wavelengths with blackbody spectra, for the red dwarf ($R_2$ = 0.36 $Ro_1$, $T_2$ = 3100 K) and white dwarf ($R_1$ = 0.01 RO, $T_1$ = 9750 K upper limit) stars at a distance d = 116 pc. The magenta line is a proposed 50 K circumbinary dust cloud. The green dash and dash-dotted lines are the emission from the fast and slow synchrotron emission models. The dash-dot-dot line is the emission from electron cyclotron maser emission (ECME). The solid green line is the sum of the ECME, the fast synchrotron emission, and the dust emission. Bayesian parameter estimation of the data between 10-1000 GHz gives a magnetic field of ≅42 G for the emission region.

[1] The George Washington University; [2] Center for Astrophysics | Harvard & Smithsonian

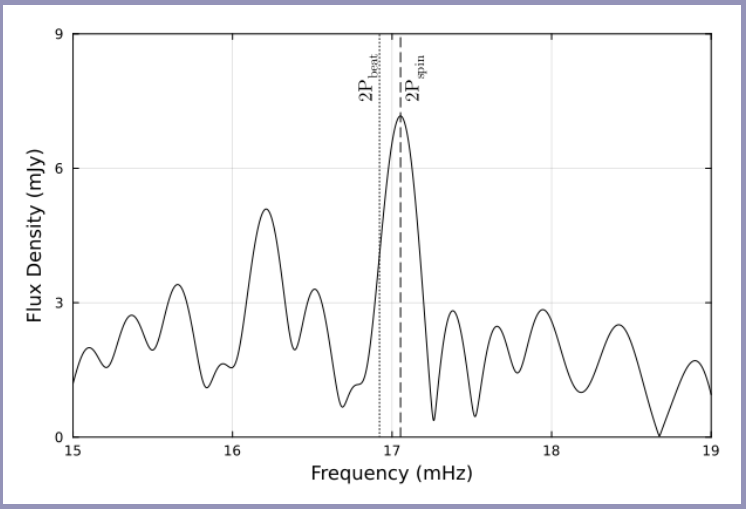


Figure 2: Periodogram of AR Sco photometry at 220 GHz. The signal at 17.053 ± 0.023 mHz with an amplitude of ≈ 6% is identified as the second harmonic of the spin period (117.12 s). The dashed vertical line is the frequency of twice the spin period and the dotted vertical line is that of twice the beat period, a difference of >5 σ.

variables that contain a magnetized (>1 MG) WD are larger than that of isolated magnetic WDs[3].

The strong spin-modulated emission due to the WD in AR Sco plus the dominant non-thermal nature of the spectral energy distribution (see Figure 1) led to the initial conclusions that magnetic interactions were powering the emission in AR Sco (Marsh *et al.* 2016; Geng *et al.* 2016; Katz 2017), in many respects resembling the emission from pulsars. Further evidence of pulsar behavior followed from optical photopolarimetric observations by Buckley *et al.* (2017), who detected spin and beat modulated linear polarization as high as 40%. They interpreted the characteristics of the polarized and non-polarized emission in terms of synchrotron emission from two different regions, one associated with the rotating magnetic field of the WD and the other caused by magneto-hydrodynamic interactions with the M-dwarf companion. A number of models have now been suggested to explain the observed behavior of AR Sco (Marsh *et al.* 2016; Geng *et al.* 2016; Katz 2017; Buckley *et al.* 2017; Takata *et al.* 2017, 2018), based on some kind of WD-RD interaction, resulting in emission from the surface or from coronal loops of the red dwarf star, its magnetosphere or possibly through an associated bow shock (Geng *et al.*, 2016; Katz 2017).

The Submillimeter Array observed AR Sco in October 2022 for one hour each at 220 and 345 GHz (Barrett *et al.* 2025). It was detected with average flux densities of 110 ± 11 mJy and 87 ± 9 mJy, respectively (Figure 1, red hexagons). The two observations helped fill a gap in the frequency spectrum between the 22 GHz Very Large Array and the 600 GHz Herschel observations. The observations showed that there is a break in the synchrotron spectrum at about 90 GHz. Bayesian model fitting of the AR Sco data between 10-1000 GHz using a synchrotron emission model with self-absorption results in a magnetic field strength of the emission region of ≅42 G and an inferred WD magnetic field of ≅15 MG, which is within the range of magnetic field strengths of Intermediate Polars (1–30 MG) that contain an asynchronously rotating WD. The inferred WD magnetic field depends on the strength of the RD magnetic field because it determines the distance of the emission region from the WD. Barrett *et al.* (2025) assume a 4 kG field for the RD, resulting in the emission region being 0.6 orbital radii from the WD. Locating the emission region is crucial to inferring the strength of the WD magnetic field and testing the WD crystallization scenario. The weak magnetic field inferred by the SMA observations imply that WD crystallization is not significant in the evolution of AR Sco. However, this result is not definitive. If the emission region is further from the WD, then its magnetic field will be stronger (~300 MG) and the WD crystallization scenario is likely to be important.

A periodogram analysis of the 220 GHz light curve shows a signal at 17.06 mHz (58.616 s) with an amplitude of 7 mJy or approximately twice the optical spin frequency of 8.53 mHz (117.258 s; see Figure 2). The SMA observations are the first direct detection of the spin period in AR Sco and demonstrates that the bulk of the synchrotron emission is associated with the WD magnetosphere and not the RD magnetosphere as seen at optical frequencies. The SMA observations support the assertion by Stanway *et al.* (2018) that there is a transition at about 10 GHz between the electron cyclotron maser emission or plasma emission at low frequencies and synchrotron emission at high frequencies.

The SMA observations of AR Sco have significantly advanced our understanding of the magnetic field of a WD pulsar by constraining the spectral energy distribution at a critical frequency of the synchrotron spectrum. The result has placed important constraints on the magnetic field of the WD, which in turn casts doubt on the WD crystallization scenario.

## REFERENCES


- S. Bagnulo et al., J. D. 2022, ApJ, 935, L12
- P. E. Barrett et al., M. 2025, ApJ, 986, 78
- D. A. H. Buckley et al. 2017, NatAs., 1, 29
- Y. Gaibor et al. 2020, MNRAS, 496, 4849
- J.-J. Geng et al. 2016, ApJL, 831, 10
- J. I. Katz 2017, ApJ, 835, 150
- T. R. Marsh et al. 2016, Natur, 537, 374
- M. R. Schreiber et al. 2021, NatAstr, 5, 648
- E. R. Stanway et al. 2018, A&A, 611, 66
- J. Takata et al. 2017, ApJ, 851, 143
- J. Takata et al. 2018, ApJ, 853, 106

# PINCHED MAGNETIC FIELDS IN THE ACCRETING HIGH-MASS PROTOCLUSTER W3 IRS5

Huei-Ru Vivien Chen[1], Qizhou Zhang[2], Tao-Chung Ching[3], Henrik Beuther[4], Kuo-Song Wang[5]

Star formation involves the interplay among gravity, turbulence, and magnetic fields across spatial scales of at least seven orders of magnitude. While gravitational contraction always facilitates star formation, magnetic fields and turbulence may either aid or hinder star formation, depending on the scale and density (e.g. McKee & Ostriker 2007). The standard paradigm for the formation of a single low-mass star (e.g., Shu *et al.* 1987) predicts that a magnetically supported molecular cloud will contract slowly through ambipolar diffusion, and eventually form a dense core that is gravitationally unstable. Alternatively, dense cores may form in a layer of swept-up neutral material on the edge of expanding HII regions when high-mass stars drive ionization and shock fronts into adjacent molecular clouds (e.g., Elmegreen & Lada 1977).

Once a dense core begins to collapse, the magnetic field lines are pulled inward under the flux freezing assumption, resulting in a pinched morphology often described as an hourglass (e.g., Li & Shu 1996). The core may fragment further as the central density increases, forming a small star cluster. Subsequent dynamical interactions among cluster members may cause the individual disk/outflow systems to deviate from their initial configurations (Zhang *et al.* 2014).

Linearly polarized emission arising from magnetically aligned dust grains is the most reliable proxy for mapping the morphology of the projected magnetic fields on the plane of the sky (Pattle *et al.* 2023). Paramagnetic grains of an elongated shape tend to spin with their minor axis aligned with the local magnetic field direction, resulting in polarized emission in the millimeter-wave bands perpendicular to the magnetic field (e.g., Andersson *et al.* 2015). Polarization studies on individual clumps have revealed a diverse morphology of the projected magnetic fields around high-mass protostars, such as an hourglass shape (Qiu *et al.* 2014; Beltrán *et al.* 2019, Saha *et al.* 2024) and spiral features dragged by rotation (Sanhueza *et al.* 2019; Beuther *et al.* 2020). Meanwhile, statistical results from surveys suggest that magnetic fields are dynamically important during the collapse and fragmentation of massive clumps (Zhang *et al.* 2014; Palau *et al.* 2021).

High-mass stars form in cluster environments and always have a significant impact on their surroundings through stellar feedback, including ionization, radiative heating, jets/outflows, and stellar winds. Such feedback may further perturb or reshape the magnetic fields (e.g. Zapata *et al.* 2024), making it challenging to interpret the observed field morphology in a core that harbors a star cluster. When a magnetic field geometry is assumed, the model field orientation, $\Psi_{mod}$, can be calculated and compared with the observed orientation, $\Psi_{obs}$. Together with the measurement uncertainties, $\sigma_{\Psi_{obs}}$, the intrinsic dispersion of the field orientation residuals, $\Delta\Psi_{obs} = \Psi_{obs} - \Psi_{mod}$, can be determined, and the Davis-Chandrasekhar-Fermi (DCF) method can be applied to estimate the field strength of the projected magnetic field component (Davis 1951; Chandrasekhar & Fermi 1953).

Located in the Perseus arm at a distance of 1.83 kpc, the luminous ($2 \times 10^5\ L_\odot$, equivalent to a single O6.5 star) infrared source W3 IRS5 is the most massive star-forming core

[1] Institute of Astronomy and Department of Physics, National Tsing Hua University; [2] Center for Astrophysics | Harvard & Smithsonian; [3] National Radio Astronomy Observatory; [4] Max Planck Institute for Astronomy; [5] Academia Sinica Institute of Astronomy and Astrophysics

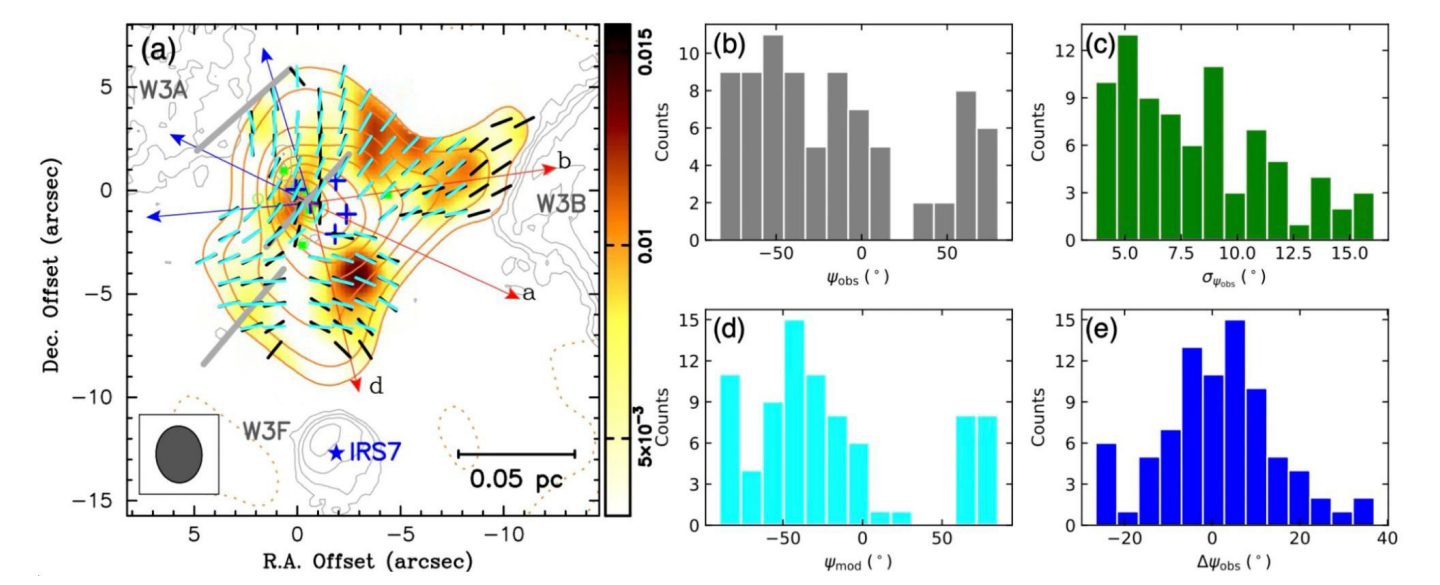


Figure 1: (a) SMA 340 GHz continuum map (red contours) overlaid on VLA 6cm continuum map (gray contours) with labels of the nearby HII regions, W3 A, W3 B, and W3 F. The blue crosses mark the positions of the five compact continuum sources previously identified (Wang et al. 2013), where SMM2 coincides with the continuum peak, and SMM1 is to the east. Line segments show the orientation of the projected magnetic field, $B_{pos}$, with the best-fit magnetic field model (cyan) overlaid on the observed $B_{pos}$ (black). The three thick line segments in gray show the large-scale magnetic field orientation measured from single-dish polarimeters. The red and blue arrows indicate known bipolar outflows (Wang et al. 2012). (b)-(e) Histograms of angular distribution for: (b) the observed P.A., $\Psi_{obs}$; (c) the measurement uncertainty, $\sigma_{\Psi_{obs}}$; (d) the P.A. of the best-fit model, $\Psi_{mod}$ ; (e) the field orientation residuals, $\Delta\Psi_{obs} = \Psi_{obs} - \Psi_{mod}$.

(715 $M_{\odot}$) in W3 Main high-mass star-forming region, and has been proposed to be a Trapezium Cluster in the making (Megeath *et al.* 2005). Early SMA observations (Wang *et al.* 2013) resolved W3 IRS5 into five compact sources, among which two (SMM1 and SMM2) coincide with known hypercompact (HC) HII regions. Using the polarimetry of the Submillimeter Array (SMA), Chen *et al.* (2025) reported a pinched magnetic field geometry in the W3 IRS5 core and estimated a projected field strength of 1.4 mG. Analyses of the energy balance and virial parameter suggest that W3 IRS5 is still accreting mass to grow. The 340 GHz polarization maps (Fig. 1) show that the projected magnetic fields, $B_{pos}$, appear organized in two parts: an hourglass centered at SMM2 and a concave shape centered at IRS7, which powers the W3 F HII region. The axis of the hourglass aligns well with the large-scale magnetic field (gray thick segments). Considering the three neighboring HII regions and the morphology of the magnetic fields, Chen *et al.* (2025) put forward a scenario for W3 IRS5. A gravitationally unstable dense core formed within a neutral gas ridge plowed by the expansion of W3 A and W3 B. The core began to contract, causing the magnetic field lines to pull inward, resulting in an hourglass morphology. The dynamic interactions between the protostars may have caused their outflow axes to become misaligned with the initial magnetic field. The subsequent expansion of W3 F, ionized by the O-type star, IRS7, perturbed the hourglass magnetic field geometry, creating the concave distortion. The impact caused by the expansion of W3 F may induce more instabilities at a later time.

## REFERENCES


- Chen et al. 2025, ApJ, 992, 199
- Andersson et al. 2015, ARA&A, 53, 501
- Shu et al. 1987, ARA&A, 25, 23
- Elmegreen & Lada 1977, ApJ, 214, 725
- McKee & Ostriker 2007, ARA&A, 45, 565
- Zhang et al. 2014, ApJ, 792, 116
- Zhang et al. 2025, ApJ, 992, 103
- Palau et al. 2021, ApJ, 912, 159
- Pattle et al. 2023, ASPC, 534, 193
- Qiu et al. 2014, ApJL, 794, L18
- Beltrán et al. 2019, A&A, 630, A54
- Sanhueza et al. 2021, ApJL, 915, L10

- Saha et al. 2024, ApJL, 972, L6
- Bik et al. 2012, ApJ, 744, 87
- Tieftrunk et al. 1997, A&A, 318, 931
- Davis 1951, PhRv, 81, 890
- Chandrasekhar & Fermi 1953, ApJ, 118, 113
- Wang et al. 2013, A&A, 558, A69
- Wang et al. 2012, ApJ, 754, 87
- Megeath et al. 2005, ApJL, 622, L141

# COMMISSIONING SMA LINEAR POLARIZATION CALIBRATION IN CASA

Joe Michail, Garrett Keating, and Ram Rao
(Center for Astrophysics | Harvard & Smithsonian)

One key priority for the SMA in recent years has been modernizing its accessibility to current standard radio astronomy calibration software, such as CASA and pyuvdata. A current and well-documented pathway for total intensity calibration exists[1], and the SMA archive can produce CASA MeasurementSet files with system-temperature-corrected visibilities. The COMPASS pipeline, which is in active stable development, will soon provide CASA-format calibration tables and/or fully calibrated data to the end user, similar to the VLA and ALMA data calibration pipelines.

However, one major missing piece of the CASA-based approach is the ability to calibrate the linear polarization data. This largely stems from current CASA limitations and how the SMA completes full polarization observations. The most critical incompatibility is calibrating the "cross-hand phase" term, which measures the phase drift between the two receivers carrying the left- and right-handed polarization feeds. There is no standard CASA function capable of carrying out this calibration, so a COMPASS function was developed to derive the necessary gain tables. Furthermore, we discovered an incompatibility in the *polcal* CASA task for the SMA's Nasmyth mount, which calculated the incorrect parallactic angles needed for instrumental polarization ("D term") calibration. An internal fix is now made to the COMPASS-exported MeasurementSet for *polcal* to derive correct D-terms.

With these developments, we published the first full-polarization SMA observation of Sgr A* calibrated completed in CASA (Michail et al., 2025; see Figure 1). The novelty and importance of these data and techniques also led us to compare the derived gain calibrator polarization properties with ALMA

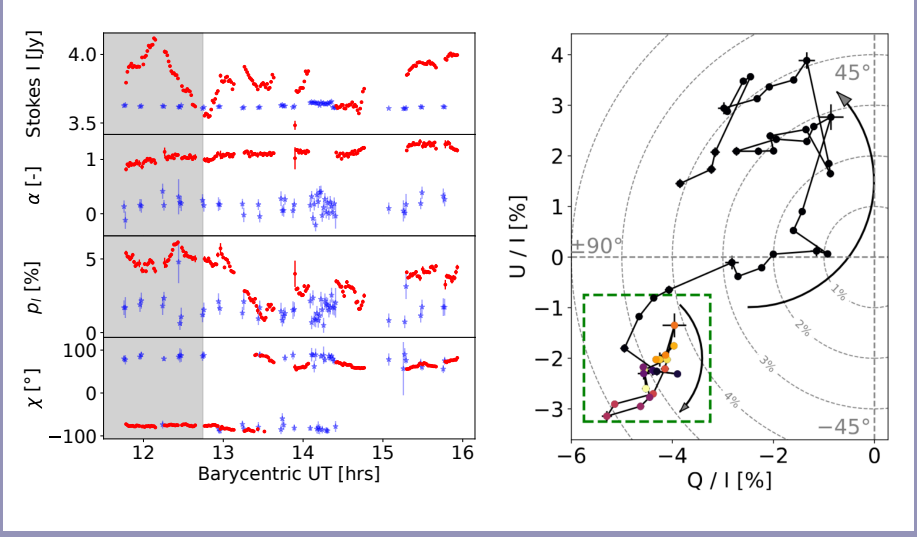


Figure 1: Sgr A* total intensity and polarized variability at 220 GHz on 6 April 2024 as observed with the SMA. Left: Light curves of Sgr A* (red) and the calibrator J1733-1304 (blue). The gray-shaded box denotes the overlap time between the SMA and JWST/MIRI instrument. The rows denote Stokes I, luminosity spectral index, debiased polarization percent, and electric vector position angle (EVPA), respectively. Right: Stokes Q vs. U plot of Sgr A* during the observation, showing clockwise-oriented motion during the JWST/MIRI observation, which is consistent with orbital motion (marked with the green dashed box). Both figures are adapted from Michail et al. (2025).

[1] https://github.com/Smithsonian/sma-data-reduction

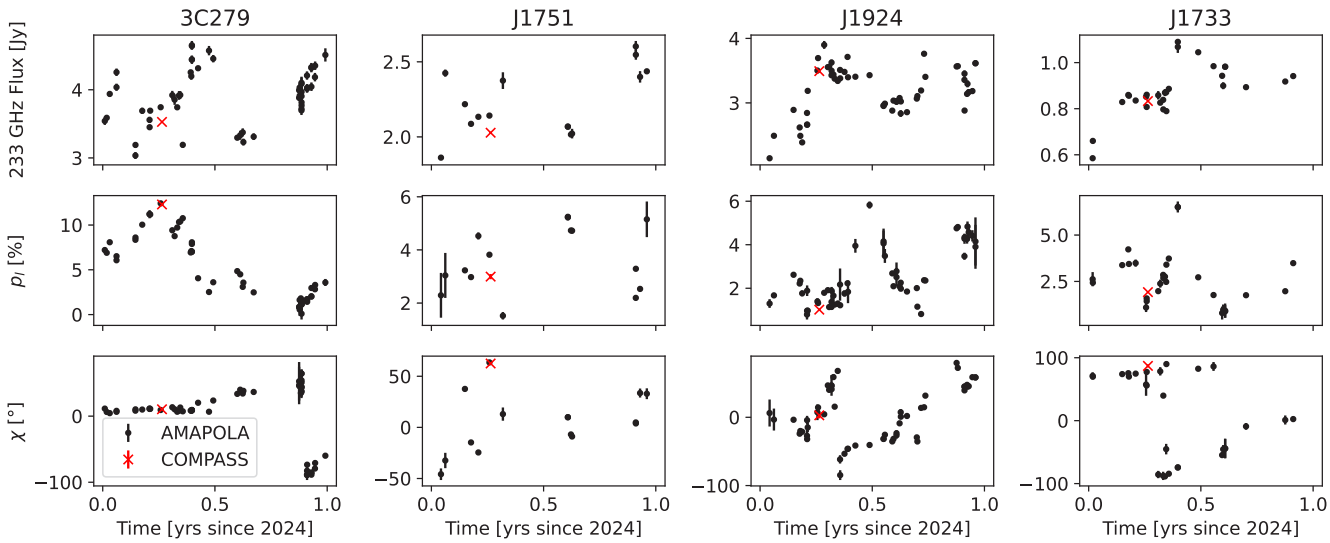


Figure 2: COMPASS-derived polarization properties (red crosses) for four calibrators in this observation, which overlap with AMAPOLA monitoring (black dots). The COMPASS/CASA results match those from AMAPOLA. We refer to Appendix A of Michail *et al.* (2025) for further details.

233 GHz monitoring observations from the AMAPOLA[2] project (Figure 2).

We are continuing to validate that the linear polarization calibration in CASA matches that from the only currently-commissioned technique (through MIRIAD and SMA-MIR) for different sources and frequencies. So far, the results are extremely promising, and we expect that we will release this calibration mode with the rest of the COMPASS suite. We plan to include extensive documentation and tutorials, similar to those in the Jupyter notebooks linked above, when polarization calibration is fully commissioned in CASA. Until then, we caution readers **not** attempt polarization calibration in CASA until these tools are released to the public. However, the parallel hand data in a full-polarization observation can be calibrated independently of the linear polarization (using the tutorials above) without concern. Observers interested in calibrating their linear polarization SMA data should contact **smarequester@cfa.harvard.edu**.

## REFERENCE


- Michail, J.M., von Fellenberg, S.D., Keating, G.K., et al. 2025, arXiv:2511.14836


[2] https://www.alma.cl/~skameno/AMAPOLA/

# SUCCESSFUL SMA SOLAR FRINGE TEST

The Submillimeter Array has achieved its first solar fringes using two recently upgraded antennas designed for submillimeter observations of the Sun, marking a major milestone for solar science at the CfA. A generous gift from Colin Masson and Leslie Masson helped to make this achievement possible. Colin is an emeritus member of the SAO Advisory Board.

The successful test was accomplished by PI Mari Paz Miralles and the Solar SMA science team—Garrett Keating, Katharine Reeves, Chad Madsen, and Mark Gurwell—whose leadership and dedication made this accomplishment possible. SMA staff in Cambridge and Hilo—Robert Christensen, Solomon Ho, Attila Kovacs, Tim Norton, Scott Paine, Ramprasad Rao, Brooks Rownd, Leslie Shirkey, Edward Tong, and Earl Townsend—as well as the CE staff—Daniel Duruski, Vanessa Marquez, Daniel Oswald, Ranjani Srinivasan, and Abigail Unger—provided outstanding technical support. Additional thanks go to Aaron Oppenheimer and Rebecca Masterson from the Project Management Office for their essential project support.

This achievement reflects the remarkable multidisciplinary expertise across the community and represents the first key step toward upgrading all eight SMA antennas to study the Sun's current active phases and future solar phenomena. Congratulations to the team!

## SMA 2026A SEMESTER CALL FOR PROPOSALS

The next Call for Standard Observing Proposals for observations with the Submillimeter Array (SMA) is for the 2026A semester with observing period nominally 16 May 2026 – 15 Nov 2026 (subject to adjustment as needed).

We are still in the planning phase for 2026A, which we expect to be partly constrained by significant infrastructure work at the SMA site. The submission deadline will likely be in early to mid-March 2026 but is not yet finalized.

As soon as the deadline is fixed, we will alert all our past users and interested parties via email and on the SMA Observer Center (SMAOC) at **http://sma1.sma.hawaii.edu/call.html**. The full Call for Proposals, with details on time available and the proposal process, will be available at least four weeks prior to the deadline, also at the SMA Observer Center.

Details on the SMA capabilities and status can be found at **http://sma1.sma.hawaii.edu/status.html**; proposal creation and submission is also done through the SMAOC at **http://sma1.sma.hawaii.edu/proposing.html**. We are happy to answer any questions and to assist in proposal submission; email sma-propose@cfa.harvard.edu with inquiries.

*Mark Gurwell, SAO Chair, SMA TAC*

## PROPOSAL STATISTICS FOR 2025B

The 2025B proposal deadline was Friday, 3 October 2025. SAO received a total of 32 standard proposals, and ASIAA received 5. SAO further received one Large Scale/Technical Development proposal. The 37 standard 2025B proposals were divided among science categories as follows:

| CATEGORY | PROPOSALS |
|---|---|
| high mass (OB) star formation, cores | 9 |
| local galaxies, starbursts, AGN | 6 |
| protoplanetary, transition, debris disks | 5 |
| low/intermediate mass star formation, cores | 4 |
| GRB, SN, high energy | 3 |
| submm/hi-z galaxies | 3 |
| other | 3 |
| evolved stars, AGB, PPN | 2 |
| galactic center | 1 |
| solar system | 1 |

We are concurrently running three accepted SAO Large Scale and one ASIAA Key Project programs.

# 2025B TRACK ALLOCATIONS BY WEATHER REQUIREMENT AND CONFIGURATION

Prior to 2025B, it was determined that to better facilitate infrastructure work, the SMA would be in COM array (max 75m baselines) for the entire semester.

Standard tracks were allocated in the following manner for different weather conditions for SAO proposals:

| PWV[1] | SAO |
|---|---|
| < 4.0mm | 35A + 43B |
| < 2.5mm | 16A + 30B |
| < 1.0mm | 0 |
| **Total** | **51A + 73B** |

[1]Precipitable water vapor required for the observations.

# TOP-RANKED 2025B SEMESTER PROPOSALS

The following is the listing of SAO proposals with at least one A-rank track allocation. ASIAA and UH have not finalized time allocation for 2025B.

### EVOLVED STARS, AGB, PPN

2025B-S006 Building an Understanding of the Intrinsic Structures of Planetary Nebulae: SMA CO Mapping of NGC 6072
*Joel Kastner, Center for Imaging Science, Rochester Institute of Technology*

### HIGH MASS (OB) STAR FORMATION, CORES

2025B-S036 Magnetic fields driving or resisting OB cluster formation
*Lennart Boehm, ESO*

### LOCAL GALAXIES, STARBURSTS, AGN

2025B-S015 Lights, Camera, Action! Filming Horizon-Scale Jet-Launching in M87 with Multi-Epoch VLBI
*Joseph Michail, Center for Astrophysics | Harvard & Smithsonian*

2025B-S018 SMAPOL: SMA Monitoring of AGNs with POLarization
*Ioannis Myserlis, Institut de Radioastronomie Milimétrique (IRAM)*

2025B-S021 *COM*pleting SMA observations to study the drastic variation of alpha_CO in M101
*Jakob den Brok, MPIA*

### OTHER

2025B-S009 Millimeter-wavelength Monitoring of a Galactic Nova
*Anna Ho, Cornell*

### PROTOPLANETARY, TRANSITION, DEBRIS DISKS

2025B-S008 A Microwave Continuum Survey of Taurus Protoplanetary Disks
*Sean Andrews, Center for Astrophysics | Harvard & Smithsonian*

# STANDARD, DDT, FILLER, LARGE SCALE AND KEY PROJECTS OBSERVED DURING 2025A

SMA Semester 2025A encompassed the period May 16, 2025 - Nov 23, 2025; listed below are projects that were at least partially completed during the semester..

### EVOLVED STARS, AGB, PPN

2025A-S001 Understanding the 3D Structures of Ring-like Planetary Nebulae: SMA CO Mapping of NGC 6871 and NGC 6563
*Joel Kastner, Center for Imaging Science, Rochester Institute of Technology*

2025A-S014 Mapping CO across the Helix Planetary Nebula (NGC 7293) with the SMA's New OTF Mode
*Joel Kastner, Center for Imaging Science, Rochester Institute of Technology*

2025A-S020 CO emission survey in X-ray emitting AGB stars
*Jaime Alonso Hernández, Centro de Astrobiología (CSIC-INTA)*

2025A-S036 The enigmatic SiO maser spectrum of ad3a-09310: a possible nascent pre-planetary nebula
*Megan Lewis, Leiden Observatory*

### GALACTIC CENTER

2025A-S037 "Round and Round She Goes": Probing hotspot orbits around Sgr A* with full polarization SMA observations
*Joseph Michail, Center for Astrophysics | Harvard & Smithsonian*

2025A-S038 What's the role of core-scale magnetic field in the CMZ?
*Xing Pan, Center for Astrophysics | Harvard & Smithsonian*

### GRB, SN, HIGH ENERGY

2022B-S046 POETS: Pursuit of Extragalactic Transients with the SMA [SAO Large Scale Project]
*Edo Berger, Harvard University*

2025A-S056 DDT: Sub-mm observations of a new mysterious extragalactic transient GRB 250702BDE
*Lauren Rhodes, McGill University*

### HIGH MASS (OB) STAR FORMATION, CORES

2023A-A012 B-fields, gravity and turbulence across multiple scales - How does the relative importance of gravity, turbulence and magnetic fields impact high-mass star and cluster formation? [ASIAA Key Project]
*Seamus Clarke, NCKU*

2025A-S018 Connecting Small and Large Scale Outflow Structures in High-Mass Star Formation
*Tatiana Rodriguez, University of Cologne*

2025A-S026 Characterizing Evolutionary Stages of Cores in High-Mass Star-Forming Regions
*Kaho Morii, University of Tokyo*

2025A-S028 Detection of Radio Recombination Lines toward the massive young star MWC 297
*Antonio Martínez-Henares, Centro de Astrobiología (CAB, CSIC-INTA)*

2025A-S053 DDT: SMA 230 GHz polarization observations of massive dense cores in Cygnus X
*Keping Qiu, School of Astronomy and Space Science, Nanjing University*

### LOCAL GALAXIES, STARBURSTS, AGN

2024B-S019 Revealing the resolved molecular gas across the M81 group
*Eric Koch, Center for Astrophysics | Harvard & Smithsonian*

2024B-S057 A complete CO(2-1) Map of M31 with SMA OTF mapping [SAO Large Scale/Technical Development Project]
*Eric Koch, Center for Astrophysics | Harvard & Smithsonian*

2025A-S034 High-frequency radio emission from Compact Symmetric Objects and its relation to X-ray obscuration
*Dominika Król, Center for Astrophysics | Harvard & Smithsonian*

2025A-S042 SMAPOL: SMA Monitoring of AGNs with POLarization
*Ioannis Myserlis, Institut de Radioastronomie Milimétrique (IRAM)*

2025A-S049 The origin of the sub-mm emission in changing-look AGN 1ES 1927+654
*Eileen Meyer, University of Maryland, Baltimore County*

2025A-S050 Investigating Observational Tracers for alpha_CO in Diverse Galactic Environments
*Yu-Hsuan Teng, Department of Astronomy, University of Maryland*

**LOW/INTERMEDIATE MASS STAR FORMATION, CORES**

2024A-A006 Probing the Hub-Filament Structures Triggered by a High-Velocity Cloud Impact
*Natsuko Izumi, Academia Sinica Institute of Astronomy and Astrophysics (ASIAA)*

2025A-S022 The first sub-1000 au scale dust spectral index map of the chemically rich shocked region L1157 B0-B1-B2
*Siyi Feng, Xiamen University (XMU)*

2025A-S039 Ultra-wide Bandwidth Observations of Stellar Flares
*Rachel Osten, STScI*

2025A-S057 DDT: Tracing Warm Molecular Gas in the M16 Pillar 1 PDR
*Marc Pound, University of Maryland*

**OTHER**

2025A-S004 Millimeter-wavelength Monitoring of a Galactic Nova
*Anna Ho, Cornell*

2025A-S035 Determining the true nature of Source 29 - a chance alignment with a star or a FIR cold-dust disk?
*Ayushi Parmar Imperial College London*

2025A-S046 SMA Observations during a Multi-Wavelength VLBA Campaign of Cygnus X-3
*Michael McCollough Center for Astrophysics | Harvard & Smithsonian*

2025A-S054 DDT: Planet-induced mm emission from the young planetary system HIP 67522
*Ekaterina Ilin, Netherlands Institute for Radio Astronomy*

**PROTOPLANETARY, TRANSITION, DEBRIS DISKS**

2025A-A003 mm flux of a newly discovered giant protoplanetary disk
*Wei-Hao Wang, ASIAA*

2025A-S013 A giant, eccentric circumbinary disk in Cepheus? Determining the origin of asymmetric sub–structure in Dracula's disk
*Joshua Lovell, Center for Astrophysics | Harvard & Smithsonian*

2025A-S024 Compact Millimeter Emission from Herbig Be Stars: Dust or Ionized Gas?
*David Wilner, Center for Astrophysics | Harvard & Smithsonian*

2025A-S033 Probing Circumstellar Dust in Young Transiting Exoplanet Systems
*Alice Booth, Center for Astrophysics | Harvard & Smithsonian*

**SOLAR SYSTEM**

2025A-S015 An SMA Spectral Survey of Venus' Mesosphere
*Alex Akins, Jet Propulsion Laboratory*

**SUBMM/HI-Z GALAXIES**

2025A-S005 The Nature of SPIRE-dropouts in the Herschel-SPIRE Deep Field
*Ayushi Parmar, Imperial College London*

2025A-S044 Elucidating the dust spectrum of WISSH QSO J1549's Companion: Towards a measurement of the hottest phase of quasar winds via the thermal Sunyaev-Zel'dovich Effect
*Kirsten Hall, Center for Astrophysics | Harvard & Smithsonian*

2025A-S048 How dense are the environments of high-z dusty star forming galaxies? Let's find out with the SMA!
*Kirsten Hall, Center for Astrophysics | Harvard & Smithsonian*

# RECENT PUBLICATIONS

**TITLE:** A Flux-limited Sample of Dusty Star-forming Galaxies from the Atacama Cosmology Telescope: Physical Properties and the Case for Multiplicity
**AUTHOR:** Hall, K. R., Hassan, J. B., Feder, R. M., Marriage, T. A., Zemcov, M., Rivera, J.
**PUBLICATION:** *The Astrophysical Journal, 996, 104*
**PUBLICATION DATE:** 01/2026
**ABSTRACT:** *https://ui.adsabs.harvard.edu/abs/2026ApJ...996..104H*
**DOI:** 10.3847/1538-4357/ae1e7a

---

**TITLE:** The complicated nature of the X-ray emission from the field of the strongly lensed hyperluminous infrared galaxy PJ1053+60 at z = 3.549
**AUTHOR:** Diaz, C. G., Wang, Q. D., Harrington, K. C., Lowenthal, J. D., Kamieneski, P. S., Jimenez-Andrade, E. F., Foo, N., Yun, M. S., Frye, B. L., Zhou, D., Vishwas, A., Yoon, I., Pampliega, B. A., Liu, D., Pascale, M.
**PUBLICATION:** *Monthly Notices of the Royal Astronomical Society, 544, 1999-2010*
**PUBLICATION DATE:** 12/2025
**ABSTRACT:** *https://ui.adsabs.harvard.edu/abs/2025MNRAS.544.1999D*
**DOI:** 10.1093/mnras/staf1851

---

**TITLE:** Probing the Physical and Chemical Characteristics of an Extremely Early Class 0 Protostar in G204.4-11.3A2-NE
**AUTHOR:** Chou, H.-I. (Ethan) ., Hirano, N., Yamaguchi, M.
**PUBLICATION:** *The Astrophysical Journal, 995, 225*
**PUBLICATION DATE:** 12/2025
**ABSTRACT:** *https://ui.adsabs.harvard.edu/abs/2025ApJ...995..225C*
**DOI:** 10.3847/1538-4357/ae197e

---

**TITLE:** Optimizing Kilonova Searches: A Case Study of the Type IIb SN 2025ulz in the Localization Volume of the Low-significance Gravitational Wave Event S250818k
**AUTHOR:** Franz, N., Subrayan, B., Kilpatrick, C. D., Hosseinzadeh, G., Sand, D. J., Alexander, K. D., Fong, W.-. fai ., Christy, C. T., Pearson, J., Laskar, T., Hsu, B., Rastinejad, J., Lundquist, M. J., Berger, E., Bostroem, K. A., Bom, C. R., Darc, P., Gurwell, M., Schimpf, S. H., Keating, G. K., Noel, P., Ransome, C., Rao, R., Santana-Silva, L., Santos, A. S., Shrestha, M., Anche, R., Andrews, J. E., Borthakur, S., Butler, N. R., Coppejans, D. L., Daly, P. N., Daniel, K. J., Duffell, P. C., Eftekhari, T., Fields, C. E., Gagliano, A. T., Golay, W. W., Grichener, A., Hamden, E. T., Hiramatsu, D., Kumar, H., Manikantan, V., Margutti, R., Paschalidis, V., Paterson, K., Reichart, D. E., Renzo, M., Salmas, K., Schroeder, G., Smith, N., Spekkens, K., Strader, J., Trilling, D. E., Vieira, N., Weiner, B., Williams, P. K. G.
**PUBLICATION:** *The Astrophysical Journal, 994, L45*
**PUBLICATION DATE:** 12/2025
**ABSTRACT:** *https://ui.adsabs.harvard.edu/abs/2025ApJ...994L..45F*
**DOI:** 10.3847/2041-8213/ae17a8

---

**TITLE:** Monitoring of 3C 286 with ALMA, IRAM, and SMA from 2006 to 2025: Stability, Synchrotron Ages, and Frequency-dependent Polarization Attributed to Core-shift

**AUTHOR:** Kam, M., Nagai, H., Kino, M., Asada, K., Kneissl, R., Agudo, I., Trippe, S., Kameno, S., Myserlis, I., Rao, R., Cho, H., Perley, R. A., Butler, B. J., Gurwell, M., Matsuoka, T., Park, J., Casadio, C., Vila Vilaro, B., Verdugo, C., Radiszcz, M., Plarre, K., Khwammai, W., Álvarez-Ortega, D., Escudero, J., Thum, C., Keating, G.

**PUBLICATION:** *The Astrophysical Journal, 994, 196*

**PUBLICATION DATE:** 12/2025

**ABSTRACT:** *https://ui.adsabs.harvard.edu/abs/2025ApJ...994..196K*

**DOI:** 10.3847/1538-4357/ae10b1

---

**TITLE:** Pinpointing the location of the γ-ray emitting region in the FSRQ 4C +01.28

**AUTHOR:** Rösch, F., Kadler, M., Ros, E., Ricci, L., Gurwell, M. A., Hovatta, T., MacDonald, N. R., Readhead, A. C. S.

**PUBLICATION:** *Astronomy and Astrophysics, 704, A143*

**PUBLICATION DATE:** 12/2025

**ABSTRACT:** *https://ui.adsabs.harvard.edu/abs/2025A&A...704A.143R*

**DOI:** 10.1051/0004-6361/202556231

---

**TITLE:** Horizon-scale variability of M87* from 2017 – 2021 EHT observations

**AUTHOR:** The Event Horizon Telescope Collaboration, Akiyama, K., Albentosa-Ruíz, E., Alberdi, A., Alef, W., Algaba, J. C., Anantua, R., Asada, K., Azulay, R., Bach, U., Baczko, A.-K., Ball, D., Baloković, M., Bandyopadhyay, B., Barrett, J., Bauböck, M., Benson, B. A., Bintley, D., Blackburn, L., Blundell, R., Bouman, K. L., Bower, G. C., Bremer, M., Brissenden, R., Britzen, S., Broderick, A. E., Broguiere, D., Bronzwaer, T., Bustamante, S., Carlos, D. F., Carlstrom, J. E., Chael, A., Chan, C.-. kwan ., Chang, D. O., Chavez, E., Chatterjee, K., Chatterjee, S., Chen, M.-T., Chen, Y., Cheng, X., Chichura, P., Cho, I., Christian, P., Conroy, N. S., Conway, J. E., Crawford, T. M., Crew, G. B., Cruz-Osorio, A., Cui, Y., Curd, B., Dahale, R., Davelaar, J., De Laurentis, M., Deane, R., Desvignes, G., Dexter, J., Dhruv, V., Dihingia, I. K., Doeleman, S. S., Dzib, S. A., Eatough, R. P., Emami, R., Falcke, H., Farah, J., Fish, V. L., Fomalont, E., Alyson Ford, H., Foschi, M., Fraga-Encinas, R., Freeman, W. T., Friberg, P., Fromm, C. M., Fuentes, A., Galison, P., Gammie, C. F., García, R., Gentaz, O., Georgiev, B., Goddi, C., Gold, R., Gómez-Ruiz, A. I., Gómez, J. L., Gu, M., Gurwell, M., Hada, K., Haggard, D., Hesper, R., Heumann, D., Ho, L. C., Ho, P., Hoak, D., Honma, M., Huang, C.-W. L., Huang, L., Hughes, D. H., Ikeda, S., Violette Impellizzeri, C. M., Inoue, M., Issaoun, S., James, D. J., Jannuzi, B. T., Janssen, M., Jeter, B., Jiang, W., Jiménez-Rosales, A., Johnson, M. D., Jorstad, S., Jones, A. C., Joshi, A. V., Jung, T., Karuppusamy, R., Kawashima, T., Keating, G. K., Kettenis, M., Kim, D.-J., Kim, J.-Y., Kim, J., Kim, J., Kino, M., Koay, J. Y., Kocherlakota, P., Kofuji, Y., Koch, P. M., Koyama, S., Kramer, C., Kramer, J. A., Kramer, M., Krichbaum, T. P., Kuo, C.-Y., La Bella, N., Lee, D., Lee, S.-S., Levis, A., Li, Z., Lico, R., Lindahl, G., Lindqvist, M., Lisakov, M., Liu, J., Liu, K., Liuzzo, E., Lo, W.-P., Lobanov, A. P., Loinard, L., Lonsdale, C. J., Lowitz, A. E., Lu, R.-S., MacDonald, N. R., Mao, J., Marchili, N., Markoff, S., Marrone, D. P., Marscher, A. P., Martí-Vidal, I., Matsushita, S., Matthews, L. D., Medeiros, L., Menten, K. M., Mizuno, I., Mizuno, Y., Montgomery, J., Moran, J. M., Moriyama, K., Moscibrodzka, M., Mulaudzi, W., Müller, C., Müller, H., Mus, A., Musoke, G., Myserlis, I., Nagai, H., Nagar, N. M., Nair, D. G., Nakamura, M., Narayanan, G., Natarajan, I., Nathanail, A., Fuentes, S. N., Neilsen, J., Ni, C., Nowak, M. A., Oh, J., Okino, H., Sánchez, H. R. O., Oyama, T., Özel, F., Palumbo, D. C. M., Paraschos, G. F., Park, J., Parsons, H., Patel, N., Pen, U.-L., Pesce, D. W., Piétu, V., Plavin, A., PopStefanija, A., Porth, O., Prather, B., Principe, G., Psaltis, D.

**PUBLICATION:** *Astronomy and Astrophysics, 704, A91*

**PUBLICATION DATE:** 12/2025

**ABSTRACT:** *https://ui.adsabs.harvard.edu/abs/2025A&A...704A..91T*

**DOI:** 10.1051/0004-6361/202555855

---

**TITLE:** Detection of Compton Scattering in the Jet of 3C 84

**AUTHOR:** Liodakis, I., Chakraborty, S., Marin, F., Ehlert, S. R., Barnouin, T., Kouch, P. M., Nilsson, K., Lindfors, E., Pursimo, T., Paraschos, G. F., Middei, R., Trindade Falcão, A., Jorstad, S., Agudo, I., Kovalev, Y. Y., Casey, J. J., Di Gesu, L., Kaaret, P., Kim, D. E., Kislat, F., Ratheesh, A., Saade, M. L., Tombesi, F., Marscher, A., José Aceituno, F., Bonnoli, G., Casanova, V., Emery, G., Escudero Pedrosa, J., Morcuende, D., Otero-Santos, J., Sota, A., Piirola, V., Bachev, R., Strigachev, A., Borman, G. A., Grishina, T. S., Hagen-Thorn, V. A., Kopatskaya, E. N., Larionova, E. G., Morozova, D. A., Savchenko, S. S.,

Shishkina, E. V., Troitskiy, I. S., Troitskaya, Y. V., Vasilyev, A. A., Zhovtan, A. V., Myserlis, I., Gurwell, M., Keating, G., Rao, R., Kang, S., Lee, S.-S., Kim, S., Yeon Cheong, W., Jeong, H.-W., Song, C., Li, S., Nam, M.-S., Álvarez-Ortega, D., Casadio, C., Angelakis, E., Kraus, A., Jormanainen, J., Fallah Ramazani, V., Chen, C.-T., Costa, E., Churazov, E., Ferrazzoli, R., Galanti, G., Khabibullin, I., O'Dell, S. L., Pacciani, L., Roncadelli, M., Roberts, O. J., Soffitta, P., Swartz, D. A., Tavecchio, F., Weisskopf, M. C., Zhuravleva, I.

**PUBLICATION:** *The Astrophysical Journal, 994, L9*
**PUBLICATION DATE:** 11/2025
**ABSTRACT:** *https://ui.adsabs.harvard.edu/abs/2025ApJ...994L...9L*
**DOI:** 10.3847/2041-8213/ae157d

---

**TITLE:** Witnessing the Violent, Merger-driven Formation of an Extremely Massive Galaxy 1.7 Gyr after the Big Bang
**AUTHOR:** Pitchford, L. K., Cairns, J., Farrah, D., Clements, D. L., Hatziminaoglou, E., Pérez-Fournon, I., Wang, L.
**PUBLICATION:** *The Astrophysical Journal, 994, 57*
**PUBLICATION DATE:** 11/2025
**ABSTRACT:** *https://ui.adsabs.harvard.edu/abs/2025ApJ...994...57P*
**DOI:** 10.3847/1538-4357/ae0292

---

**TITLE:** Unveiling blazar synchrotron emission: A multiwavelength polarimetric study of high-synchrotron and low-synchrotron peaked populations
**AUTHOR:** Capecchiacci, S., Liodakis, I., Middei, R., Kim, D. E., Di Gesu, L., Agudo, I., Agís-González, B., Arbet-Engels, A., Blinov, D., Chen, C.-T., Ehlert, S. R., Gau, E., Heckmann, L., Hu, K., Jorstad, S. G., Kaaret, P., Kouch, P. M., Krawczynski, H., Lindfors, E., Marin, F., Marscher, A. P., Myserlis, I., O'Dell, S. L., Pacciani, L., Paneque, D., Perri, M., Puccetti, S., Saade, M. L., Tavecchio, F., Tennant, A. F., Traianou, E., Weisskopf, M. C., Wu, K., Aceituno, F. J., Bonnoli, G., Casanova, V., Emery, G., Escudero, J., Morcuende, D., Otero-Santos, J., Sota, A., Piirola, V., Borman, G. A., Kopatskaya, E. N., Larionova, E. G., Morozova, D. A., Shishkina, E. V., Savchenko, S. S., Vasilyev, A. A., Grishina, T. S., Troitskiy, I. S., Zhovtan, A. V., McCall, C., Jermak, H. E., Steele, I. A., Bachev, R., Strigachev, A., Imazawa, R., Sasada, M., Fukazawa, Y., Kawabata, K. S., Uemura, M., Mizuno, T., Nakaoka, T., Tochihara, S., Akai, T., Akitaya, H., Berdyugin, A. V., Kagitani, M., Kravtsov, V., Poutanen, J., Sakanoi, T., Álvarez-Ortega, D., Casadio, C., Kang, S., Lee, S.-S., Kim, S., Cheong, W. Y., Jeong, H.-W., Song, C., Li, S., Nam, M.-S., Gurwell, M., Keating, G., Rao, R., Angelakis, E., Kraus, A., Benke, P., Debbrecht, L., Eich, J., Eppel, F., Gokus, A., Hämmerich, S., Heßdörfer, J., Kadler, M., Kirchner, D., Paraschos, G. F., Rösch, F., Schulga, W.

**PUBLICATION:** *Astronomy and Astrophysics, 703, A19*
**PUBLICATION DATE:** 11/2025
**ABSTRACT:** *https://ui.adsabs.harvard.edu/abs/2025A&A...703A..19C*
**DOI:** 10.1051/0004-6361/202555392

---

**TITLE:** The First Radio-bright Off-nuclear Tidal Disruption Event AT 2024tvd Reveals the Fastest-evolving Double-peaked Radio Emission
**AUTHOR:** Sfaradi, I., Margutti, R., Chornock, R., Alexander, K. D., Metzger, B. D., Beniamini, P., Duran, R. B., Yao, Y., Horesh, A., Farah, W., Berger, E., A. J., N., Cendes, Y., Eftekhari, T., Fender, R., Franz, N., Green, D. A., Hammerstein, E., Lu, W., Wiston, E., Bernstein, Y., Bright, J., Christy, C. T., Cruz, L. F., DeBoer, D. R., Golay, W. W., Goodwin, A. J., Gurwell, M., Keating, G. K., Laskar, T., Miller-Jones, J. C. A., Pollak, A. W., Rao, R., Siemion, A., Sheikh, S. Z., Shoval, N., van Velzen, S.

**PUBLICATION:** *The Astrophysical Journal, 992, L18*
**PUBLICATION DATE:** 10/2025
**ABSTRACT:** *https://ui.adsabs.harvard.edu/abs/2025ApJ...992L..18S*
**DOI:** 10.3847/2041-8213/ae0a26

---

**TITLE:** Pinched Magnetic Fields in the High-mass Protocluster W3 IRS5
**AUTHOR:** Chen, H.-R. V., Zhang, Q., Ching, T.-C., Beuther, H., Wang, K.-S.
**PUBLICATION:** *The Astrophysical Journal, 992, 199*
**PUBLICATION DATE:** 10/2025
**ABSTRACT:** *https://ui.adsabs.harvard.edu/abs/2025ApJ...992..199C*
**DOI:** 10.3847/1538-4357/adfbec

---

**TITLE:** Detailed Microwave Continuum Spectra from Bright Protoplanetary Disks in Taurus
**AUTHOR:** Painter, C., Andrews, S. M., Chandler, C. J., Ueda, T., Wilner, D. J., Long, F., Macias, E., Carrasco-Gonzalez, C., Chung, C.-Y., Liu, H. B., Birnstiel, T., Hughes, A. M.
**PUBLICATION:** *The Open Journal of Astrophysics, 8, 134*
**PUBLICATION DATE:** 09/2025
**ABSTRACT:** *https://ui.adsabs.harvard.edu/abs/2025OJAp....8E.134P*
**DOI:** 10.33232/001c.144268

---

**TITLE:** Modeling the Multiwavelength Emission of 3C 279 during the 14 yr Fermi-LAT Era
**AUTHOR:** Mohana A, K., Gupta, A. C., Fan, J., Sahakyan, N., Raiteri, C. M., Cui, L., Lähteenmäki, A., Gurwell, M., Tornikoski, M., Villata, M.
**PUBLICATION:** *The Astrophysical Journal, 989, 125*
**PUBLICATION DATE:** 08/2025
**ABSTRACT:** *https://ui.adsabs.harvard.edu/abs/2025ApJ...989..125M*
**DOI:** 10.3847/1538-4357/adec77

---

**TITLE:** SMA and NOEMA Reveal Asymmetric Substructure in the Protoplanetary Disk of IRAS 23077+6707
**AUTHOR:** Lovell, J. B., Trapman, L., Monsch, K., Andrews, S. M., Booth, A. S., Keating, G. K., Ueda, T., Wilner, D. J.
**PUBLICATION:** *The Astrophysical Journal, 989, 69*
**PUBLICATION DATE:** 08/2025
**ABSTRACT:** *https://ui.adsabs.harvard.edu/abs/2025ApJ...989...69L*
**DOI:** 10.3847/1538-4357/ade392

---

**TITLE:** IXPE Observations of the Blazar Mrk 501 in 2022: A Multiwavelength View
**AUTHOR:** Lisalda, L., Gau, E., Krawczynski, H., Tavecchio, F., Liodakis, I., Gokus, A., Rodriguez Cavero, N., Nowak, M., Negro, M., Middei, R., Perri, M., Puccetti, S., Jorstad, S. G., Agudo, I., Marscher, A. P., Ag'is-Gonz'alez, B., Berdyugin, A. V., Bernardos, M. I., Blinov, D., Bonnoli, G., Borman, G. A., Bourbah, I. G., Casadio, C., Casanova, V., Castro-Tirado, A. J., Fern'andez-Garc'ia, E., Garc'ia-Comas, M., Grishina, T. S., Hakala, P., Hovatta, T., Hu, Y. D., Husillos, C., Escudero, J., Jormanainen, J., Aceituno, F. J., Kagitani, M., Kiehlmann, S., Kontopodis, E., Kopatskaya, E. N., Kouch, P. M., Kravtsov, V., L"ahteenm"aki, A., Larionova, E. G., Lindfors, E., Mandarakas, N., Marchini, A., Masiero, J. R., Mawet, D., Max-Moerbeck, W., Morozova, D. A., Myserlis, I., Nilsson, K., Panopoulou, G. V., Pearson, T. J., Readhead, A. C. S., Reeves, R., Romanopoulos, S., Sakanoi, T., Salom'e, Q., Savchenko, S. S., Skalidis, R., Sota, A., Syrj"arinne, I., Tinyanont, S., Tornikoski, M., Troitskaya, Y. V., Troitskiy, I. S., Vasilyev, A. A., Vervelaki, A., Zhovtan, A. V., Antonelli, L. A., Bachetti, M., Baldini, L., Baumgartner, W. H., Bellazzini, R., Bianchi, S., Bongiorno, S. D., Bonino, R., Brez, A., Bucciantini, N., Capitanio, F., Castellano, S., Cavazzuti, E., Chen, C., Ciprini, S., Costa, E., De Rosa, A., Del Monte, E., Gesu, L. D., Lalla, N. D., Marco, A. D., Donnarumma, I., Doroshenko, V., Dovčiak, M., Ehlert, S. R., Enoto, T., Evangelista, Y., Fabiani, S., Ferrazzoli, R., Garcia, J. A., Gunji, S., Gurwell, M., Hayashida, K., Heyl, J., Iwakiri, W., Kaaret, P., Karas, V., Keating, G., Kislat, F., Kitaguchi, T., Kolodziejczak, J. J., La Monaca, F., Latronico, L., Maldera, S., Manfreda, A., Marin, F., Marinucci, A., Marshall, H. L., Massaro, F., Matt, G., Mitsuishi, I., Mizuno, T., Muleri, F., Ng, C., O'Dell, S. L., Omodei, N., Oppedisano, C., Papitto, A., Pavlov, G. G., Peirson, A. L., Pesce-Rollins, M., Petrucci, P., Pilia, M., Possenti, A., Poutanen, J., Ramsey, B. D., Rankin, J., Rao, R., Ratheesh, A., Roberts, O. J., Romani, R. W., Sgrò, C., Slane, P., Soffitta, P., Spandre, G., Swartz, D. A., Tamagawa, T., Taverna, R., Tawara, Y., Tennant, A. F., Thomas, N. E., Tombesi, F., Trois, A., Tsygankov, S. S., Turolla, R., Vink, J., Weisskopf, M. C., Wu, K., Xie, F., Zane, S.
**PUBLICATION:** *Monthly Notices of the Royal Astronomical Society,*
**PUBLICATION DATE:** 07/2025
**ABSTRACT:** *https://ui.adsabs.harvard.edu/abs/2025MNRAS.tmp.1094L*
**DOI:** 10.1093/mnras/staf1122

---

**TITLE:** OGLE-2002-BLG-360: A dusty anomaly among red nova remnants
**AUTHOR:** Steinmetz, T., Kamiński, T., Melis, C., Blagorodnova, N., Gromadzki, M., Menten, K., Su, K.
**PUBLICATION:** *Astronomy and Astrophysics, 699, A316*
**PUBLICATION DATE:** 07/2025
**ABSTRACT:** *https://ui.adsabs.harvard.edu/abs/2025A&A...699A.316S*
**DOI:** 10.1051/0004-6361/202554261

---

**TITLE:** A Two-week IXPE Monitoring Campaign on Mrk 421
**AUTHOR:** Maksym, W. P., Liodakis, I., Saade, M. L., Kim, D. E., Middei, R., Di Gesu, L., Kiehlmann, S., Matzeu, G., Agudo, I., Marscher, A. P., Ehlert, S. R., Jorstad, S. G., Kaaret, P., Marshall, H. L., Pacciani, L., Perri, M., Puccetti, S., Kouch, P. M., Lindfors, E., Aceituno, F. J., Bonnoli, G., Casanova, V., Escudero, J., Gómez, J. L., Agís-González, B., Husillos, C., Morcuende, D., Otero-Santos, J., Sota, A., Piirola, V., Imazawa, R., Sasada, M., Fukazawa, Y., Kawabata, K. S., Uemura, M., Mizuno, T., Nakaoka, T., Akitaya, H., McCall, C., Jermak, H. E., Steele, I. A., Borman, G. A., Grishina, T. S., Hagen-Thorn, V. A., Kopatskaya, E. N., Larionova, E. G., Morozova, D. A., Savchenko, S. S., Shishkina, E. V., Troitskiy, I. S., Troitskaya, Y. V., Vasilyev, A. A., Zhovtan, A. V., Myserlis, I., Gurwell, M., Keating, G., Rao, R., Pauley, C., Angelakis, E., Kraus, A., Berdyugin, A. V., Kagitani, M., Kravtsov, V., Poutanen, J., Sakanoi, T., Kang, S., Lee, S.-S., Kim, S.-H., Cheong, W. Y., Jeong, H.-W., Song, C., Blinov, D., Shablovinskaya, E., Antonelli, L. A., Bachetti, M., Baldini, L., Baumgartner, W. H., Bellazzini, R., Bianchi, S., Bongiorno, S. D., Bonino, R., Brez, A., Bucciantini, N., Capitanio, F., Castellano, S., Cavazzuti, E., Chen, C.-T., Ciprini, S., Costa, E., De Rosa, A., Del Monte, E., Di Lalla, N., Di Marco, A., Donnarumma, I., Doroshenko, V., Dovčiak, M., Enoto, T., Evangelista, Y., Fabiani, S., Ferrazzoli, R., Garcia, J. A., Gunji, S., Hayashida, K., Heyl, J., Iwakiri, W., Karas, V., Kislat, F., Kitaguchi, T., Kolodziejczak, J. J., Krawczynski, H., La Monaca, F., Latronico, L., Maldera, S., Manfreda, A., Marin, F., Marinucci, A., Massaro, F., Matt, G., Mitsuishi, I., Muleri, F., Negro, M., Ng, C.-Y., O'Dell, S. L., Omodei, N., Oppedisano, C., Papitto, A., Pavlov, G. G., Peirson, A. L., Pesce-Rollins, M., Petrucci, P.-O., Pilia, M., Possenti, A., Ramsey, B. D., Rankin, J., Ratheesh, A., Roberts, O. J., Romani, R. W., Sgró, C., Slane, P., Soffitta, P., Spandre, G., Swartz, D. A., Tamagawa, T., Tavecchio, F., Taverna, R., Tawara, Y., Tennant, A. F., Thomas, N. E., Tombesi, F., Trois, A., Tsygankov, S. S., Turolla, R., Vink, J., Weisskopf, M. C., Wu, K., Xie, F., Zane, S.
**PUBLICATION:** *The Astrophysical Journal, 986, 230*
**PUBLICATION DATE:** 06/2025
**ABSTRACT:** *https://ui.adsabs.harvard.edu/abs/2025ApJ...986..230M*
**DOI:** 10.3847/1538-4357/adce6b

---

**TITLE:** The Role of Pressure in the Structure and Stability of GMCs in the Andromeda Galaxy
**AUTHOR:** Lada, C. J., Forbrich, J., Krumholz, M. R., Keto, E.
**PUBLICATION:** *The Astrophysical Journal, 986, 12*
**PUBLICATION DATE:** 06/2025
**ABSTRACT:** *https://ui.adsabs.harvard.edu/abs/2025ApJ...986...12L*
**DOI:** 10.3847/1538-4357/adcf9d

---

Photo by Brooks Rownd

The Submillimeter Array (SMA) is a pioneering radio-interferometer dedicated to a broad range of astronomical studies including finding protostellar disks and outflows; evolved stars; the Galactic Center and AGN; normal and luminous galaxies; and the solar system. Located on Maunakea, Hawaii, the SMA is a collaboration between the Smithsonian Astrophysical Observatory and the Academia Sinica Institute of Astronomy and Astrophysics.


SUBMILLIMETER ARRAY
Center for Astrophysics | Harvard & Smithsonian
60 Garden Street, MS 78
Cambridge, MA 02138 USA
www.cfa.harvard.edu/sma/

SMA HILO OFFICE
645 North A'ohoku Place
Hilo, Hawaii 96720
Ph. 808.961.2920
Fx. 808.961.2921
sma1.sma.hawaii.edu

ACADEMIA SINICA INSTITUTE
OF ASTRONOMY & ASTROPHYSICS
11F of Astronomy-Mathematics Building,
AS/NTU, No. 1, Sec. 4, Roosevelt Road
Taipei 10617
Taiwan R.O.C.
www.asiaa.sinica.edu.tw/